optica

Mapping complex mode volumes with cavity perturbation theory: supplementary material

K. G. COGNÉE,[1,2] W. YAN,[1] F. LA CHINA,[3] D. BALESTRI,[3] F. INTONTI,[3] M. GURIOLI,[3] A. F. KOENDERINK,[2] AND P. LALANNE[1,*]

[1]LP2N, Institut d'Optique, CNRS, Univ. Bordeaux, Talence, 33400, France
[2]Center for Nanophotonics, AMOLF, Science Park 104, 1098XG, Amsterdam The Netherlands
[3]LENS, University of Florence, Sesto Fiorentino, 50019, Italy
*Corresponding author: philippe.lalanne@institutoptique.fr

Published 28 February 2019

This document provides supplementary information to "Mapping complex mode volumes with cavity perturbation theory," https://doi.org/10.1364/OPTICA.6.000269. It includes complementary results and discussions pertaining to the main article. Section 1 discusses details of the reliability of the ΔQ-measurements. Next, is a formal comparison of the classical perturbation formula of Eqs. (1) and (2) in the main article, followed by a study of the accuracy of Eq. (2) for predicting resonance shifts, and finally an analytical study of the domain of validity of Eq. (2) that leads to upper bounds for the maximum perturber strength.

1. Experimental details

We use the tip to excite the embedded InAs QD with a c.w. laser at 780 nm and, for every tip position, we measure the QD photoluminescence spectrum. At room temperature, the spectrum covers more than 100 nm. It exhibits a Lorentzian peak for each cavity resonance. Due to the interaction with the tip, $\mathrm{Re}(\tilde{\omega})$ and $\mathrm{Im}(\tilde{\omega})$ are both modified. By fitting the spectra for every tip position, we obtain the $\Delta\lambda$ and Q maps reported in Fig. 1.

The feedback mechanism of the SNOM is able to maintain the tip on the sample surface at constant height, whenever the sample is flat. In photonic crystal cavities, it forces the tip to follow the topography and then, when the tip is on an air pore, the tip height is reduced by few tens of nm. The measure of the tip-height map, see Fig. S1a, allows us to reconstruct, a posteriori, the perturbation map with a spatial alignment of a few tens of nanometers, which is needed for a comparison with theoretical prediction. The z-scan is then performed by moving the sample vertically with steps of 20 nm. During the vertical scan, the tip is maintained at a constant height. Then, after each z-scan, the sample is repositioned thank to the feedback mechanism to keep the spatial alignment, and then is moved in the (x, y) plane.

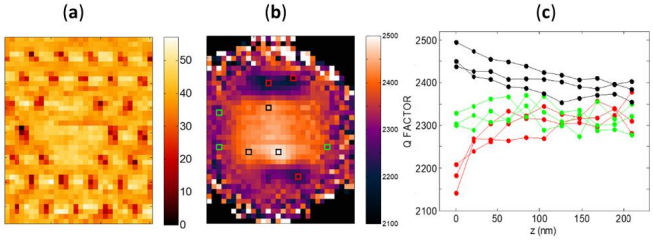

Fig. S1 (a) Topography map. (b) Corresponding Q-variation map. The colored squares represent several tip locations. (c) Q-variation as a function of the offseted distance $z - d_{min}$ between the tip and the photonic-crystal membrane. The black, green and red curves are obtained for tip locations shown in (c) with the squares of the same colors.

In order to detect possible systematic errors in the z-scan (such as sample/tip drift), we repeated the z-scan several times for different (x, y) locations. An example is shown in Figs. S1b-c. Figure S1b reports the Q map at $z = 0$ for three A points (red squares), three B points (black squares) and three C points (green squares), all located at quite different position. Figure S1c reports the Q-variation for every points. All the data converge to a common value with similar trends, denoting the reliability of the presented data.

Finally, we address the repeatability of the SNOM measurements to detect possible artefacts. Figure S2 shows three different maps of the Q-factor obtained with the same tip during three different days. The data comparison conclusively evidences a quantitative agreement between the three sets of data.

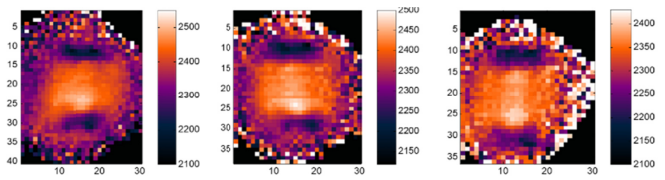

Fig. S2 Three different maps of the Q-variation induced by the SNOM tip measured for three different days without changing the tip.

2. Formal comparison of Eqs. (1) and (2)

The main difference between Eqs. (1) and (2) resides in the replacement of $\tilde{\mathbf{E}} \cdot \tilde{\mathbf{E}}^*$ product by the unconjugated product $\tilde{\mathbf{E}} \cdot \tilde{\mathbf{E}}$. In order to clarify the impact of the replacement for high-Q microcavities, we consider perturbations formed by deep-subwavelength isotropic dielectric perturbers (volume V_p, permittivity $\Delta\varepsilon + \varepsilon_b$) that are introduced into a background material of permittivity ε_b. In the static limit, the perturbers act as point isotropic electric dipoles, with a polarizability proportional to their perturber volume $\alpha = \alpha' V_p$, α' being a dimensionless coefficient. For spherical perturbers at optical frequencies, $\alpha' = \frac{3\Delta\varepsilon}{\Delta\varepsilon + 3\varepsilon_b}$ with $-1.5 < \alpha' < 3$ for perturbers with a positive permeability. Replacing α in Eq. (2), and assuming that α' is a real number, we get

$$\frac{\mathrm{Re}(\Delta\tilde{\omega})}{\mathrm{Re}(\tilde{\omega})} \approx -\frac{\alpha'}{2}\left[\mathrm{Re}\left(\frac{V_p}{\tilde{V}}\right) - \frac{1}{2Q}\mathrm{Im}\left(\frac{V_p}{\tilde{V}}\right)\right], \tag{S1a}$$

$$\frac{\mathrm{Im}(\Delta\tilde{\omega})}{\mathrm{Im}(\tilde{\omega})} \approx -\frac{\alpha'}{2}\left[\mathrm{Re}\left(\frac{V_p}{\tilde{V}}\right) + 2Q\ \mathrm{Im}\left(\frac{V_p}{\tilde{V}}\right)\right]. \tag{S1b}$$

For high-Q photonic cavities, $\mathrm{Im}(\tilde{\mathbf{E}}) \ll \mathrm{Re}(\tilde{\mathbf{E}})$ and $\mathrm{Re}\left(\frac{V_p}{\tilde{V}}\right) \approx \frac{V_p}{V} \gg \frac{1}{2Q}\mathrm{Im}\left(\frac{V_p}{\tilde{V}}\right)$ (remember that V is the approximate mode volume defined in Eq. (1)), so that Eq. (S1a) reduces to

$$\mathrm{Re}(\Delta\tilde{\omega}) \approx -\omega_0 \alpha' \frac{V_p}{V}, \tag{S2a}$$

which is exactly the shift predicted by Eq. (1). Note that this conclusion does not hold for low-Q plasmonic resonators. Quite the contrary, the imaginary part $\mathrm{Im}\left(\frac{V_p}{\tilde{V}}\right)$ cannot be neglected in general in Eq. (S1b). Even for our microcavity, Fig. 2a evidences that the imaginary part dominates over the real part $\frac{1}{2Q}\mathrm{Re}\left(\frac{V_p}{\tilde{V}}\right)$, i.e.,

$$\mathrm{Im}\left(\frac{V_p}{\tilde{V}}\right) \gg \frac{1}{2Q}\mathrm{Re}\left(\frac{V_p}{\tilde{V}}\right) \text{ and}$$

$$\mathrm{Im}(\Delta\tilde{\omega}) \approx -\frac{\alpha'}{2}\mathrm{Re}(\tilde{\omega})\ \mathrm{Im}\left(\frac{V_p}{\tilde{V}}\right). \tag{S2b}$$

This mathematically justifies why Eq. (1) fails at predicting $\mathrm{Im}(\Delta\tilde{\omega})$.

3. Accuracy of Eq. (2) to predict resonance shifts

The main text focuses on the prediction of perturbation-induced quality-factor changes, ΔQ, which is the novelty of the work. For the sake of completeness, we have performed a similar study for the resonance shift, whose main result are summarized in Figs. S3 and S4. The conclusion for our cavity geometry is that Eq. (2) is as accurate to predict wavelength shifts, as it is at predicting Q-changes. We believe that this result represents a strong evidence of the great added value brought by Eq. (2) for high-Q cavities.

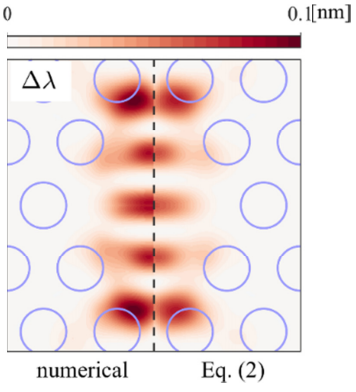

Fig. S3 Validation of Eq. (2) for the resonance wavelength shift $\Delta\lambda$ by comparison with exact numerical data obtained by solving the perturbed cavity. All simulations are obtained with the same structure and perturber as in the Fig. 2 in the main text.

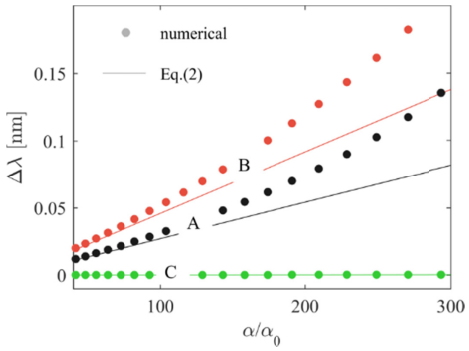

FIG. S4 Study of the validity range of Eq. (2) for predicting resonance wavelength shifts $\Delta\lambda$ by comparison with fully-numerical data obtained by solving the perturbed cavity. The perturber polarizability α is normalized by α_0, the static polarizability of a silica sphere with 10-nm radius in air. Three perturber positions, 30 nm above the semiconductor membrane, are considered; they are labelled as "A", "B", "C", corresponding to the same position in Fig. 1(e) in the main text.

4. Validity domain of Eq. (2)

As evidence by Fig. 2c in the main text, Eq. (2) is exact in the limit of infinitely small perturbations. In this Section, we would like to quantify under which condition Eq. (2) may be approximately valid and used with confidence to predict both resonance shifts and ΔQ-changes.

To obtain a qualitative insight into the domain of validity of Eq. (2), we start from the exact Eqs. (3) and (4), insert Eq. (4) into Eq. (3), annul the driving field ($\mathbf{E}_b = 0$), then perform a Taylor expansion with respect to α up to the second order, and obtain

$$\frac{\Delta\tilde{\omega}}{\tilde{\omega}} \approx -\alpha\tilde{\mathbf{E}}_{\boldsymbol{N}} \cdot [\mathbf{I} + \alpha\mu_0\tilde{\omega}^2\delta\mathbf{G}] \cdot \tilde{\mathbf{E}}_{\boldsymbol{N}}. \tag{S3}$$

The second term inside the bracket, $\alpha\mu_0\omega^2\delta\mathbf{G}$ gathers the contribution of all other modes that contribute to the mode density at the cavity, except for the cavity mode that is singled out by $\tilde{\mathbf{E}}_N$. In the limit that this contribution is negligible, Eq. (S3) simply reduces to Eq. (2) in the main text. Accordingly, the validity of Eq. (2) requires that

$$\|\alpha\mu_0\tilde{\omega}^2\delta\mathbf{G}\|_\infty \ll 1, \tag{S4}$$

where the operation $\|\cdots\|_\infty$ represents the infinite norm of a matrix.

Though Eq. (S4) formally quantifies the domain of validity of Eq. (2), it is difficult to extract more information, since $\delta\mathbf{G}$ is a 3×3 symmetric matrix containing 6 different components. To bypass this difficulty, we make the approximation $\delta\mathbf{G} \approx \delta G\mathbf{I}$, with $\delta G \equiv \mathrm{Tr}(\delta\mathbf{G})/3$, i.e., neglecting the vectorial character of δG, where $\mathbf{I}$ represents the identity matrix, and further assume α is real, i.e., neglecting radiation loss and material absorption of the perturber. Under these approximations, we compare $\Delta\tilde{\omega}$ predicted from Eq. (SI-2) and Eq. (2), and derive that the dominant conditions for Eq. (2) to accurately predict $\mathrm{Re}(\Delta\tilde{\omega})$ and $\mathrm{Im}(\Delta\tilde{\omega})$ are respectively

$$|\alpha| \ll \alpha_r \ \text{ and } |\alpha| \ll \alpha_i, \tag{S5}$$

where α_r and α_i are given by

$$\alpha_r = \min\left\{\left|\frac{1}{\mu_0\,\mathrm{Re}(\omega^2\delta G)}\right|, \left|\frac{1}{\mu_0\,\mathrm{Im}(\omega^2\delta G)}\right| \left|\frac{\mathrm{Re}(\tilde{V}^{-1})}{\mathrm{Im}(\tilde{V}^{-1})}\right|\right\}, \quad \text{(S6a)}$$

$$\alpha_i = \min\left\{\left|\frac{1}{\mu_0\,\mathrm{Re}(\omega^2\delta G)}\right|, \left|\frac{1}{\mu_0\,\mathrm{Im}(\omega^2\delta G)}\right| \left|\frac{\mathrm{Im}(\tilde{V}^{-1})}{\mathrm{Re}(\tilde{V}^{-1})}\right|\right\}. \quad \text{(S6b)}$$

Note that, to derive Eqs. (S5)-(S6), we have used the relations, $\mathrm{Re}(\tilde{V}^{-1}) \gg \frac{1}{2Q}\mathrm{Im}(\tilde{V}^{-1})$ and $\mathrm{Im}(\tilde{V}^{-1}) \gg \frac{1}{2Q}\mathrm{Re}(\tilde{V}^{-1})$ which are valid for high-Q cavities.

The expressions of α_r and α_i can be further simplified by first noting that (1) $\left|\frac{\mathrm{Re}(\tilde{V}^{-1})}{\mathrm{Im}(\tilde{V}^{-1})}\right| \gg 1$ for high-Q cavity and (2) we generally have $|\mathrm{Re}(\omega^2\delta G)| \gg \mathrm{Im}(\omega^2\delta G)|$ (as confirmed by numerical simulations[1]) for perturbers placed in the near-field of the cavity. We finally obtain simplified expressions for α_r and α_i

$$\alpha_r = \left|\frac{1}{\mu_0\,\mathrm{Re}(\omega^2\delta G)}\right|, \quad \text{(S7a)}$$

$$\alpha_i = \min\left\{\alpha_r, \left|\frac{1}{\mu_0\,\mathrm{Im}(\omega^2\delta G)}\right| \left|\frac{\mathrm{Im}(\tilde{V}^{-1})}{\mathrm{Re}(\tilde{V}^{-1})}\right|\right\}. \quad \text{(S7b)}$$

As a numerical example, we consider the two perturber positions A and C in Fig. 1a for which noticeable ΔQ and $\Delta\lambda$ changes are observed. We numerically find that $\alpha_r = \alpha_i = 665\alpha_0$ at position A, and $\alpha_r = 702\alpha_0$ at position B and $\alpha_i = 541\alpha_0$ at position C, where α_0 denotes the static polarizability of a silica sphere with 10-nm radius in air like in the main text. For both cases, α_r and α_i have similar values, and this a posteriori explains why Eq. (2) is as accurate to predict wavelength shifts, as it is at predicting Q-changes.

[1] $\delta\mathbf{G}$, and then δG, has been computed with COMSOL Multiphysics. A reasonable estimate for the typical magnitude of δG is that it is essentially the non-resonant contribution to the full system Green function [scattered part strictly] on top of which the resonant cavity mode adds. The non-resonant background is of the same order as the Green function of free space for a perturber placed outside the cavity.